

Evaluation of a second-generation monoenergetic reconstruction algorithm for lesion contrast and venous invasion in pancreatic ductal adenocarcinomas

S.-Q. ZHUO¹, H.-L. MA¹, L.-Z. LIU¹, G.-Y. RUAN¹, C.-B. XIE², W.-J. HUANG¹, G.-J. YANG³, Z.-P. LI¹, S.-H. ZENG¹

¹Department of Medical Imaging, State Key Laboratory of Oncology in South China, Collaborative Innovation Center for Cancer Medicine, Sun Yat-sen University Cancer Center, Guangzhou, China

²Department of Cancer Prevention Research, State Key Laboratory of Oncology in South China, Collaborative Innovation Center for Cancer Medicine, Sun Yat-sen University Cancer Center, Guangzhou, China

³Department of Radiology, The Third Affiliated Hospital of Kunming Medical University, Yunnan Cancer Hospital, Kunming, China

Shuiqing Zhuo and Huali Ma contributed equally to this work

Abstract. – OBJECTIVE: At lower energy levels, virtual monochromatic imaging by dual-energy computed tomography improves lesion attenuation but produces greater image noise with the conventional monoenergetic reconstruction algorithm (Mono). Recently, a second-generation algorithm (Mono+) was introduced to overcome this limitation. We compared the quality of images obtained with these algorithms and investigated the optimal energy selection for pancreatic ductal adenocarcinomas (PDACs).

PATIENTS AND METHODS: Image data from 54 PDAC cases were generated at 40, 50, 60, 70, and 80 keV using Mono and Mono+. Image quality was objectively assessed by comparing the signal-to-noise ratios (SNRs), noise, and the contrast-to-noise ratios (CNRs) at different keV levels and between these algorithms at the same keV level. Lesion conspicuity and venous invasion were subjectively assessed.

RESULTS: For Mono, the mean pancreas and tumour SNRs peaked at 70 keV ($p < 0.001$). The noise increased as the energy level decreased ($p < 0.001$). CNR_{tumour} remained unchanged. For Mono+, the mean pancreas SNR peaked at 40 keV ($p < 0.001$). The mean tumour SNR and noise remained unchanged. The tumour CNRs were highest at 40 keV (4.9 times the CNR of Mono 40 keV, $p < 0.001$). Subjectively, lesion conspicuity was best at Mono+ 40 keV ($p < 0.001$) and it showed higher diagnostic performance levels on venous invasion assessment against Mono.

CONCLUSIONS: Mono+ produced better image quality, and 40 keV is recommended for the diagnosis of PDAC.

Key Words:

Dual-energy computed tomography, Pancreatic ductal adenocarcinoma, Virtual monochromatic imaging.

Abbreviations

CNR_{tumour}: Contrast-to-noise ratio of the lesion-to-pancreas contrast; CT: Computed tomography; DECT: Dual-energy CT; IVC: Inferior vena cava; NCCN: National Comprehensive Cancer Network; PDAC: Pancreatic ductal adenocarcinoma; PV: Portal vein; ROI: Region of interest; SNR_{panc}: Signal-to-noise ratio of the pancreas; SNR_{tumour}: Signal-to-noise ratio of the tumour; SMV: Superior mesenteric vein.

Introduction

Pancreatic ductal adenocarcinoma (PDAC) is one of the most life-threatening tumours and is often diagnosed at an advanced stage, wherein complete surgical resection (R0 resection) is difficult, as adjacent abdominal vessels are markedly invaded. According to the National Comprehensive Cancer Network (NCCN) *Clinical Practice Guidelines*, the surgical procedure for PDAC is based on the location of the tumour and

its relationship with blood vessels¹. Radiographic characteristics suggesting infiltrative invasion of the portal vein (PV), superior mesenteric vein (SMV), and inferior vena cava (IVC) are the main unfavourable factors influencing R0 resection. Preoperative computed tomography (CT) imaging is critical because of its ability to demonstrate venous invasion from the tumour with fast acquisition of contrast-enhanced scans and the availability of multiplanar reformatting. However, tumour conspicuity is the most intractable problem on conventional CT imaging, which may hinder accurate evaluation.

Dual-energy CT (DECT) has been receiving increasing clinical attention in recent years. One of its benefits is that it can be used to create virtual monochromatic images at arbitrary energies from the polychromatic low-keV and high-keV data. CT images can be synthesised using different monochromatic x-ray beams with the first-generation conventional monoenergetic reconstruction algorithm (Mono). Tumour conspicuity can be improved at lower scanning voltages, as higher atomic numbers produce higher image density to enhance tumour-to-tissue contrast^{2,3}. However, at lower keV levels, the background noise increases and outweighs the benefit of higher tissue attenuation⁴. In an effort to reduce this background noise limitation, a second-generation monoenergetic reconstruction algorithm (Mono+) has been introduced. Mono+ produces images with a combination of high attenuation at low photon energies and lower image noise at higher photon energies by using a spatial frequency-based technique⁵. Frellesen et al⁶ on Mono+ have shown promising results, suggesting that this novel reconstruction algorithm may overcome the limitations produced by noise and improve image quality to enable better visualisation of pancreatic tumours. However, venous invasion was not investigated in these studies, some of which included patients with multiple pancreatic tumours⁷⁻⁹. Virtual monochromatic images at lower energy levels can increase tissue attenuation; therefore, we assumed that Mono+ can improve lesion contrast and the accuracy of venous invasion evaluation.

In this study, we first compared image quality, with a focus on lesion-to-pancreas contrast, in an image series at energy levels of 40-80 keV (in 10-keV increments) using Mono and Mono+ and investigated the optimal energy selections. Second, the diagnostic accuracy of venous invasion was further assessed at these optimal selections in

patients with postsurgical pathologically proven diagnoses confirming whether there was venous involvement or not.

Patients and Methods

Patients

This was a retrospective imaging data analysis that included patients with suspected pancreatic tumours based on clinical symptoms, such as abdominal pain, weight loss, and an elevated serum CA199 level or patients in whom a pancreatic tumour had been detected by a previous imaging study between June 2017 and March 2019 at a single centre. Figure 1 shows the flowchart of the patient inclusion procedure. Among 201 patients, 54 that were ultimately confirmed to have PDAC on the basis of endoscopic ultrasound-guided fine-needle aspiration or post-surgical pathology were included in the image quality analysis. Twenty-five of these patients who had pathological confirmation of presence or absence of venous invasion were sub-grouped and their data used in the venous invasion assessment. DECT scanning is a routine workup in the assessment of underlying abdominal tumours. This investigation was approved by our institutional Ethics Committee, and the need for informed consent was waived.

Computed Tomography Scanning Protocol

All scanning was performed on a dual-source CT scanner (Somatom Force, Siemens Healthineers, Forchheim, Germany). All patients were placed in a supine position. Acquisitions were performed in the cranial-to-caudal direction with breath hold. A standard unenhanced scan and triple-phasic enhanced scans, which included an arterial phase, a pancreatic parenchymal phase (PPP), and a delayed phase, were obtained from the level of the diaphragm to the bifurcation of the abdominal aorta. After the unenhanced scan, an intravenous bolus injection of non-ionic contrast media (350 mg/mL [1.5 mL/kg]) was administered at a rate of 4 mL/s through the median cubital vein. A circular region of interest (ROI) with an area of 1 mm² was placed in the aorta 2 cm below the diaphragm. A threshold of 100 Hounsfield units (HU) was set. Arterial phase acquisition was initiated 7 s after the trigger. The scanning duration was approximately 5-7 s. Acquisition of the PPP and the delayed phase was initiated automatically at 20 s and 3 min lat-

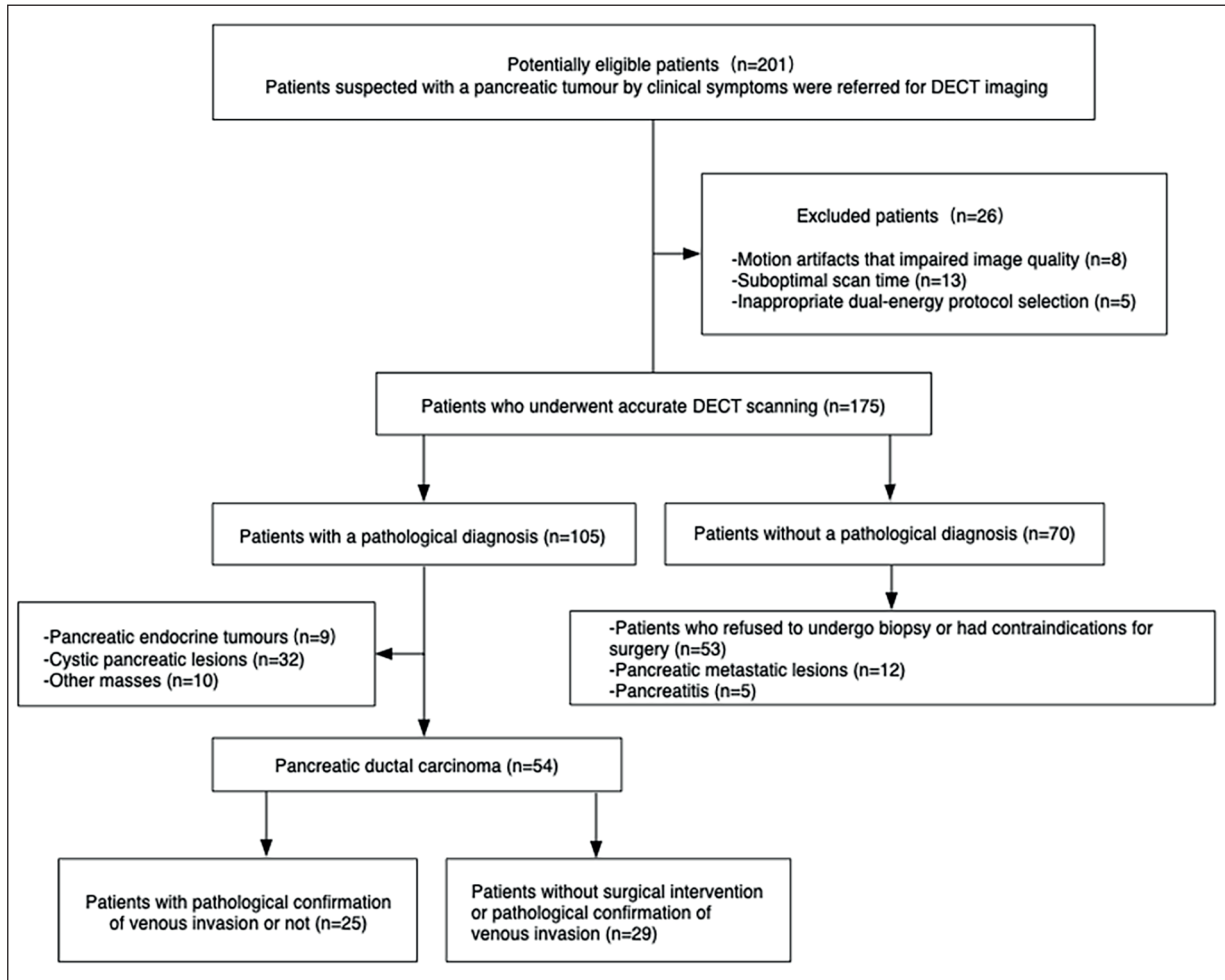


Figure 1. Flowchart of the patient inclusion process. (DECT, dual-energy computed tomography).

er, respectively, when arterial phase acquisition was accomplished. Only images in the PPP were obtained using the dual-energy mode with tube A at 100 KV/ref250 mAs and tube B at 150 KV/ref125 mAs with tin filtration. Other scanning parameters were as follows: exposure technique, CARE Dose4D automatic exposure control to regulate tube current; rotation time, 0.5 s; pitch, 1; collimation, 2 mm × 192 mm × 0.6 mm; and reconstruction thickness, 1 mm.

Image Reconstruction

Image data of dual-energy at the PPP were generated and reconstructed into pure 100 KV and Sn150 KV datasets on the CT console. These datasets were transferred to the workstation and processed using dedicated dual-energy monochromatic software (syngo.via, version VB20, Siemens Healthcare, Munich, Germany). Mono

and Mono+ images were created at virtual photon energies of 40 keV, 50 keV, 60 keV, 70 keV, and 80 keV by nonlinear blending.

Image Quality Analysis

Objective Analysis

Objective analysis was conducted by a radiologist with 5 years of experience in abdominal CT imaging. The image series were displayed simultaneously on the comparative reading section of syngo.via on the workstation. Regions of interest of ≥1 mm² were placed in areas of air, normal pancreatic tissue, and tumour on the same axial slice of pure 100 KV (Figure 2). The copy-and-paste function was applied to the rest of the image series, which included Mono 40 keV, 50 keV, 60 keV, 70 keV, and 80 keV, and Mono+ 40

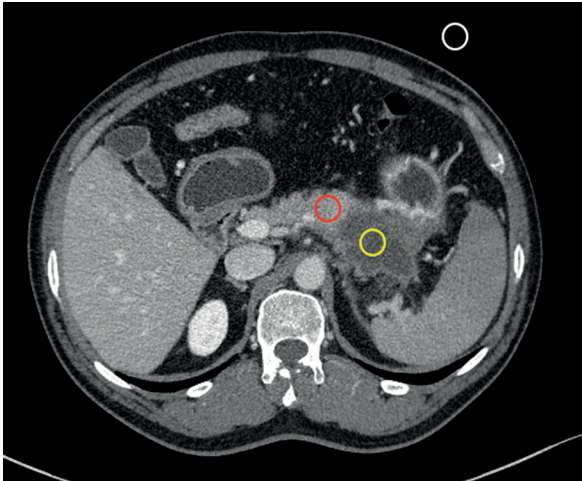


Figure 2. The placement of the regions of interest in the areas of air (*white circle*), normal pancreatic tissue (*red circle*), and the tumour (*yellow circle*).

keV, 50 keV, 60 keV, 70 keV, and 80 keV. These measurements were conducted three times, and the results were averaged to ensure reliability. If the lesion was iso-intense, the ROI was set according to the other reconstructed series that could better display it. Image noise was defined as the standard deviation of attenuation measured in the extracorporeal air (SD). The signal-to-noise ratios of the pancreas (SNR_{panc}) and the tumour (SNR_{tumour}) were calculated using the equation $SNR = ROI/SD$. The contrast-to-noise ratio for the lesion-to-pancreas contrast was calculated using the equation $CNR_{tumor} = (ROI_{panc} - ROI_{tumour})/SD$.

For tumour size measurements, the largest diameter of the hypo-attenuated mass was measured on the axial plane of sole 100 KV images.

Subjective Analysis

Lesion Conspicuity Assessment

A different radiologist, with 8 years of experience in abdominal CT imaging, independently assessed image quality using syngo.via on the workstation. The 10 series were displayed in random order in axial orientation and with a slice thickness of 1 mm. The window width and window level were initially set at 400 HU and 40 HU, respectively. The reader scrolled through and adjusted the window settings freely. Image quality ratings were agreed upon by a reader who was trained beforehand with a training set. Le-

sion conspicuity was assessed on a 5-point scale with the highest score indicating the best image quality. The scale was based on the optimal image contrast and on image noise, as follows: 1 = “excellent with no noise”; 2 = “good with minimal noise”; 3 = “satisfactory with mild noise”; 4 = “deficient with moderate noise”; 5 = “nondiagnostic with severe noise.”

Venous Invasion Assessment

The presence of venous invasion, including of the PV, SMV, and IVC, was assessed by the reader who performed the aforementioned objective imaging quality analysis in a 3-month interval. Twenty-five patients with pathological confirmation of presence or absence of venous invasion were included in the assessment, and the images at the keV levels that resulted in the highest lesion conspicuity values using the two algorithms were selected for the assessment. Images were displayed in a random order.

CT imaging findings suggesting venous invasion were classified into three types using Loyer’s criteria as a reference. Type A: Absence of invasion (fat plane or pancreatic parenchyma separates the tumour from adjacent vessels); Type B: Probable presence of invasion (hypodense tumour inseparable from vessels (points of contact either forms a convexity or concavity against vessels); Type C: Definite presence of invasion (hypodense tumour encircles or occludes adjacent vessels).

Statistical Analysis

All statistical analyses were conducted with Prism 7.0 (GraphPad Software Inc., La Jolla, CA, USA). Continuous variables are reported as mean \pm standard deviation. The Kruskal–Wallis test with Bonferroni post-hoc correction was used for objective and subjective comparison of image quality measurements. The sensitivity and specificity for the two algorithms for venous invasion diagnosis were also calculated. For all analyses, $p < 0.05$ was considered statistically significant.

Results

Thirty-one and 23 masses were detected at the pancreatic head and body-tail, respectively. The tumour size (expressed as the mean \pm standard deviation) was 3.50 ± 1.24 cm (range, 2.0–5.3 cm). Two masses were iso-intense and the other 52 were hypointense on 100 KV images in the PPP.

Table I presents an overview of the objective measurements. Figure 3 presents the differences across the image series.

For Mono, the mean SNR_{panc} and SNR_{tumour} values showed nearly parabolic curves and peaked at 70 keV. As the energy level decreased, the SNR values also decreased. There was a significant difference ($p < 0.001$, Table I) between each two incremental energy levels lower than 60 keV for the SNR_{panc} and SNR_{tumour}. In addition, the mean noise showed a decay curve. As the energy level was lowered, the noise increased; it peaked at 40 keV, where it was statistically significantly different from all other energy levels ($p < 0.001$). When the effects of the SNR and noise were combined, there were no differences in CNR_{tumour} at any energy level.

However, on Mono+, these variables showed different curves. The mean SNR_{panc} slightly increased as the energy level decreased; it peaked at Mono+ 40 keV, where it was significantly different from that at the 70 keV or 80 keV energy levels, but not from that at Mono+ 50 keV ($p < 0.001$). The mean SNR_{tumour} and noise did not significantly differ among energy levels. Combining the effects from SNR and noise, CNR_{tumour} showed evident decay curves. As the energy level decreased, the values sharply increased; they peaked at Mono+ 40 keV, being statistically different from those at all other energy levels ($p < 0.001$).

When comparing the values between Mono and Mono+ at the same energy level, higher SNR_{panc} and SNR_{tumour} were produced on Mono+

below the level of 70 keV ($p < 0.001$). Noise was replenished on Mono+ at lowered energy levels, at approximately one-fifth of that on Mono at the 40 keV energy level (Table I; $p < 0.001$). CNR_{tumour} was higher on Mono+ below the energy level of 70 keV, at 4.9 times the value on Mono at the 40 keV energy level (Table I; $p < 0.001$).

The lesion conspicuity assessment results are presented in Table II and Figure 4. Lesion conspicuity rated best on Mono+ 40 keV among the two imaging datasets; however, it was not statistically significantly different from that on Mono+ 50 keV ($p < 0.001$). Within the Mono dataset, it rated best on Mono 60 keV ($p < 0.001$).

The venous invasion assessment results of the 25 pathologically confirmed cases are shown in Table III and Figure 5.

There was isolated PV invasion in none of the cases (0/25) and four cases were classified into type C with respect to combined PV/SMV involvement in the two algorithms, with 100% sensitivity and specificity.

In total, 13 and 12 cases were classified into Type B or C with respect to isolated SMV invasion on Mono 60 keV and Mono+ 40 keV, respectively. One case was misdiagnosed as invasion on Mono 60 keV for iso-attenuating lesions seemingly compressing the adjacent vein (Figures 5A, 5B). The sensitivity and specificity of Mono 60 keV vs. Mono+ 40 keV were 100% and 92.9% vs. 100% and 100%, respectively.

Regarding isolated IVC invasion, there was diagnostic uncertainty in three cases with insufficient homogeneous enhancement. For the

Table I. Objective measurements of the signal-to-noise ratio, noise, and the contrast-to-noise ratio.

	keV	SNR _{panc}	SNR _{tumor}	Noise	CNR _{tumor}
Mono	40	2.60 (0.78)*	0.98 (0.49)*	45.57 (8.27)*	5.24 (2.18)
	50	3.30 (0.97)*	1.29 (0.63)*	28.80 (6.81)*	5.83 (2.37)
	60	4.50 (1.30)*	2.19 (1.61)*	17.31 (3.24)*	6.61 (4.14)
	70	5.69 (1.45)	2.90 (0.93)	10.52 (1.68)*	6.93 (3.52)
	80	5.13 (1.54)	2.55 (0.92)	10.02 (2.09)	6.30 (2.84)
Mono+	40	6.71 (1.62) ^Δ	2.86 (1.35)	9.44 (1.48)	25.48 (11.13)*
	50	6.66 (1.65) ^Δ	2.91 (1.31)	9.54 (1.47)	16.86 (7.01)*
	60	6.38 (1.55)	2.95 (1.32)	9.47 (1.69)	12.13 (5.52)*
	70	5.90 (1.73)	2.96 (0.95)	9.74 (1.48)	7.49 (3.65)*
	80	5.86 (1.42)	2.90 (1.12)	9.48 (1.70)	6.96 (3.16)

SD, standard deviation; SNR, Signal-to-noise ratio; CNR, Contrast-to-noise ratio; Mono, monoenergetic imaging algorithm; Mono+, second-generation monoenergetic imaging algorithm; SNR_{panc}, SNR of pancreas; SNR_{tumor}, SNR of tumor; CNR_{tumor}, CNR of the lesion-to-pancreas contrast. Variables are expressed as the mean (SD). *The value is statistically significantly different from the values at the other energy levels ($p < 0.001$). **The value is statistically significantly different from the values of Mono+ 50 keV, 60 keV, 70 keV, and 80 keV ($p < 0.001$). ^ΔThe value is statistically significantly different from Mono+ 40 keV vs. 70 keV or 80 keV, and different from Mono+ 50 keV vs. 70 keV or 80 keV ($p < 0.001$).

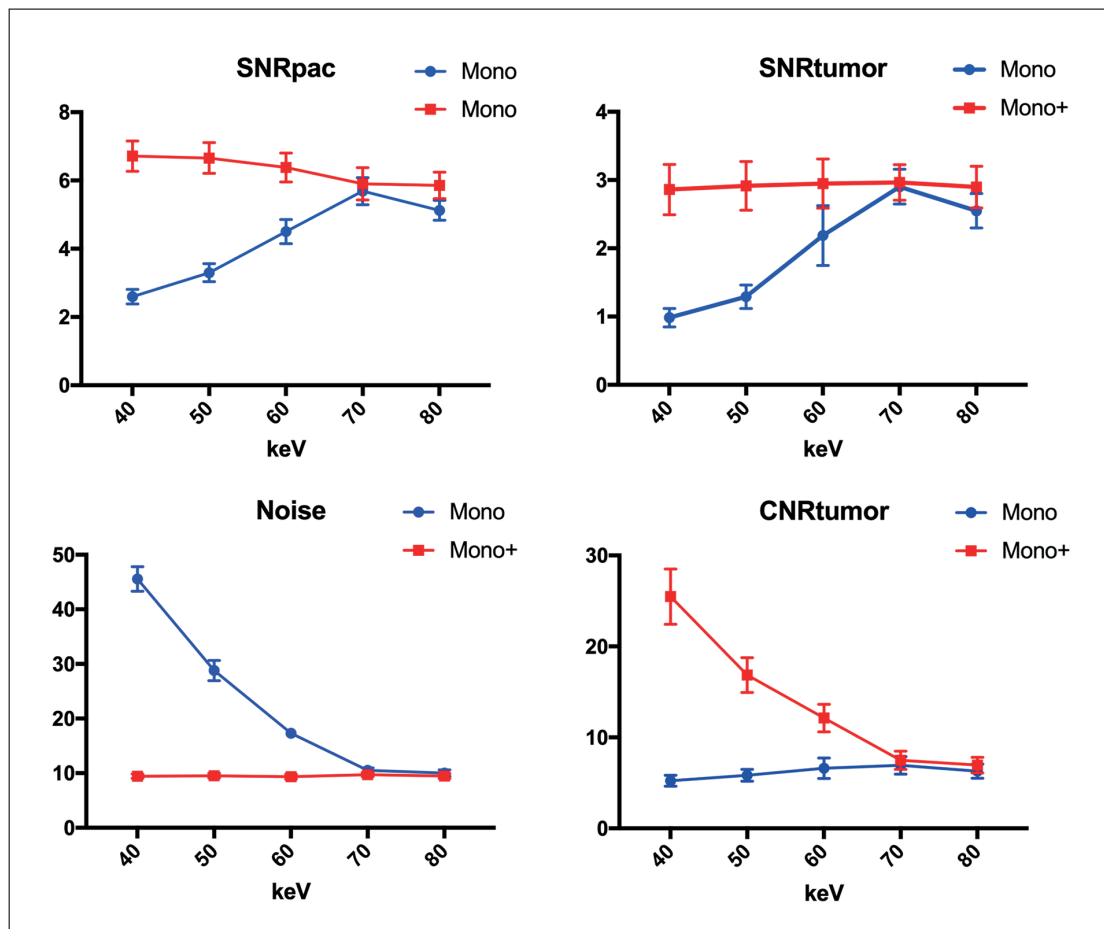


Figure 3. The boxplots represent differences across image series from virtual monochromatic images at energy levels from 40 keV to 80 keV by Mono and Mono+ algorithms for SNR_{panc}, SNR_{tumour}, noise, and CNR_{tumour} (Mono, monoenergetic imaging algorithm; Mono+, second-generation monoenergetic imaging algorithm; SNR, signal-to-noise ratio; SNR_{panc}, SNR of the pancreas; SNR_{tumour}, SNR of the tumour; CNR, contrast-to-noise ratio; CNR_{tumour}, CNR of the lesion-to-pancreas contrast).

other 22 cases, a total of seven and eight cases were classified into Type B or C on Mono 60 keV and Mono+ 40 keV, respectively. One case of invasion was missed on Mono 60 keV due to image noise (Figures 5C, 5D). The sensitivity and specificity of Mono 60 keV vs. Mono+ 40 keV were 88.9% and 100% vs. 100% and 100%, respectively.

Discussion

DECT scanning is a promising technique that produces dual x-rays by two separate tubes at low and high voltages to achieve material decomposition. Spectral images, especially iodine, fat, and osseous images, can be produced. Before its application, imaging was polychromatic and

Table II. Subjective ratings of lesion conspicuity.

	40	50	60	70	80	40+	50+	60+	70+	80+
Lesion conspicuity	3.35 (0.62)	3.63 (0.56)	4.02 (0.53)	3.80 (0.66)	3.57 (0.54)	4.43 (0.57)	4.24 (0.58)	3.96 (0.58)	3.72 (0.56)	3.72 (0.53)

The data are presented as the mean (standard deviation). “+” Indicates these levels were assessed using the second-generation monoenergetic imaging algorithm (Mono+).

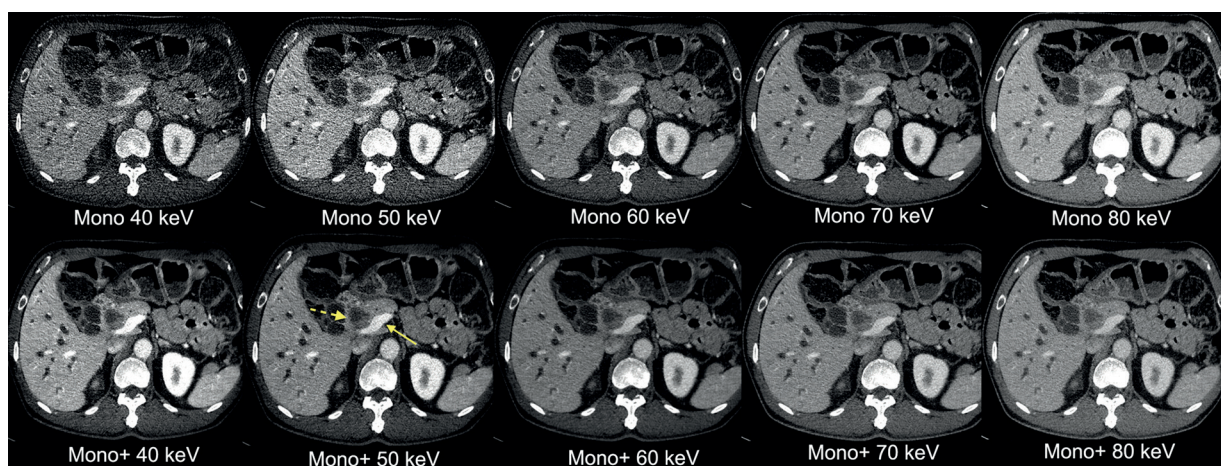


Figure 4. The same image slice shows the PDAC lesion at the head of the pancreas by virtual monochromatic imaging at different energy levels. Unilateral compression on the root of the portal vein (*arrow*) by the tumour (*arrow with dotted line*) is best visualised using Mono+ 50 keV for better tumour-to-pancreas contrast. This patient underwent pancreaticoduodenectomy with regional PV resection, and PV invasion was confirmed pathologically (Mono, monoenergetic imaging algorithm; Mono+, second-generation monoenergetic imaging algorithm).

with average attenuation from a single tube. The DECT technique can produce a series of virtual monochromatic images in different ranges of energies. Monochromatic images at lower energy can increase lesion-to-tissue contrast and vessel opacification^{2,10,11}. Owing to the desmoplastic re-

action and their infiltrative growth characteristics, PDACs are mostly iso-attenuated or hypo-attenuated on enhanced images, which make it difficult to discern them from adjacent normal pancreatic tissues with conventional CT imaging¹². Studies on improving pancreatic imaging are ongoing

Table III. Venous invasion classification from Mono and Mono+ at the keV energy level with the best lesion conspicuity.

	Type	PV	SMV	PV+SMV	IVC
Mono 60 keV	A	0	12	21	15
	B	0	5	0	6
	C	0	8	4	1
Mono+ 40 keV	A	0	13	21	14
	B	0	5	0	7
	C	0	7	4	1

The data are presented as number of cases. PV, portal vein; SM, superior mesenteric vein; IVC, inferior vena cava.

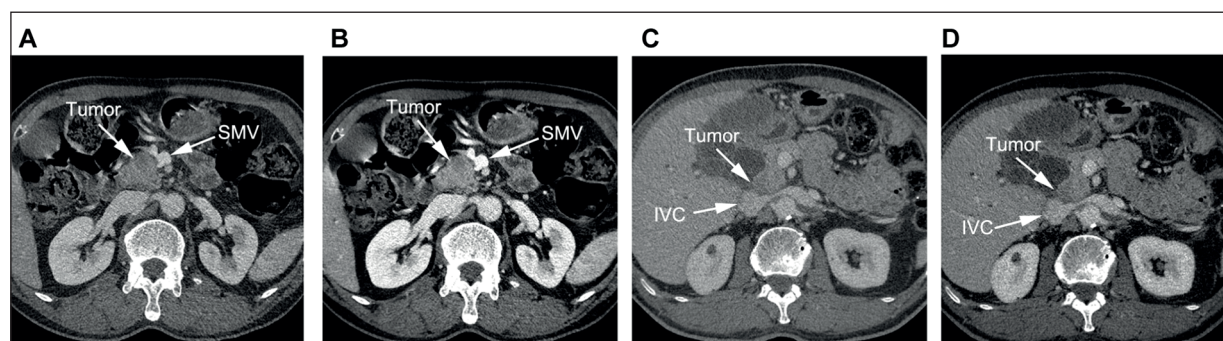


Figure 5. A pancreatic tumour was inconspicuous, and the adjacent flattening superior mesenteric vein (SMV) was misdiagnosed as invasion on the Mono 60 keV image (A). The normal pancreatic parenchyma was better shown between the tumour and the SMV on the Mono+ 40 keV image (B). A case with confirmed inferior vena cava (IVC) invasion. The tumour invasion was less conspicuous on the Mono 60 keV image (C) than on the Mono+ 40 keV image (D).

and recent studies have increasingly focused on pancreatic virtual monochromatic imaging. This imaging technique can better detect PDAC, especially small and iso-attenuated lesions, and allows good reader agreement in diagnosis¹³⁻¹⁵.

Computed virtual monochromatic imaging of DECT scans at lower kiloelectron volt levels can increase x-ray attenuation of materials with a high atomic number such as iodine (which improves iodine contrast)^{2,11}. However, when using the conventional monoenergetic imaging reconstruction algorithm (i.e., Mono), image noise will simultaneously increase at lower kiloelectron volt levels, which may ultimately lower the CNR⁴. To overcome these image noise limitations, an advanced monoenergetic imaging reconstruction algorithm (i.e. Mono+) was developed¹⁶. By means of a frequency-split technique, the benefits of high attenuation from low kiloelectron volt images and high spatial frequency from optimal kiloelectron volt images can be combined to achieve a higher CNR. The advantage of Mono+ in improving lesion contrast, vascular attenuation, and image quality has been demonstrated by recent studies⁶⁻⁹. The optimal energy level on conventional Mono with regard to CNR is approximately 60-70 keV. Lower energy levels would lead to a sharp increase in noise. However, higher image quality at 40 keV was shown to be possible using Mono+, on the basis of a phantom study⁸. This capability was also demonstrated in pancreatic imaging. A preliminary clinical study on 22 cases of pancreatic masses by Hardie et al⁹ showed that attenuation on the pancreatic parenchyma and lesion was much higher on Mono+ 55 keV images than on linearly blended 120 kV images at the PPP, although a mild increase in noise also occurred, which resulted in a significantly greater CNR. Bellini et al⁷ also demonstrated that noise was significantly lower and the pancreas-to-muscle CNR was significantly higher for energy levels below 70 keV when using Mono+, and the CNR was maximised at Mono+ 40 keV. To the best of our knowledge, the only study that focused on pancreatic-to-lesion CNR of confirmed pancreatic carcinoma by using Mono+ was conducted by Frellesen et al⁶. They demonstrated that the pancreatic-to-lesion CNR peaked at Mono+ 40 keV. However, subjective image reading suggested that the energy level of 55 keV by Mono+ would achieve the best image quality. Our study showed that in normal pancreatic and tumour tissue, Mono+ 40 keV was the best energy level to attain a higher SNR with

the least noise, ultimately resulting in the highest CNR. In addition, subjective qualitative analysis suggested that lesion conspicuity and venous invasion were rated best at energy levels of 40 keV when using Mono+.

Mono+ is a promising algorithm that improves vessel visualisation. Bhosale et al⁴ compared image quality between Mono images obtained using the DECT scanning technique and images obtained using conventional single energy acquisition. The energy level of 70 keV was identified as the best for visualising tumour extension and vascular invasion. Schabel et al¹⁶ proved the advantage of Mono+ in overcoming the noise limitations and confirmed Mono+ 40 keV as the best energy level for depicting intrahepatic veins under poor contrast conditions. However, few studies have been conducted on Mono+ with regard to vascular invasion of PDAC. Most patients are diagnosed at an advanced stage; vascular involvement is frequent. On the basis of the NCCN criteria, resectability is highly dependent on pre-operative evaluation of tumour contact with the adjacent vessels. The Society of Abdominal Radiology and the American Pancreatic Association recommend examining patients using biphasic CT, which contains a PPP and a portal venous phase (obtained 40-50 s and 65-70 s, respectively, after the intravenous injection of contrast medium), as a routine workup for evaluating arterial and venous involvement in the former phase, as well as liver metastases in the latter phase¹⁷. However, at the portal venous phase, venous contrast is inferior to arterial contrast. Moreover, liver metastases may not be well visualised because peak enhancement of the liver parenchyma would not have been achieved. Thus, the delayed phase was reserved in our study. We aimed to explore the influence of the newer algorithm on lesion conspicuity and on venous invasion evaluation at the PPP.

In this study, on the basis of an average score of 4.43 and 4.24, Mono+ at the energy levels of 40 keV and 50 keV rated best for lesion conspicuity and showed significant improvement over Mono. The diagnostic accuracy for venous invasion improved at Mono+ 40 keV.

This study has several limitations. First, the effect of body size was not studied, although signal attenuation and image noise may differ among individuals. Recent studies have demonstrated that sufficient tube current modulation by an automated exposure control, such as CARE Dose 4D, which was applied in this

research, can eliminate variability. Second, we only focused on image quality assessment. We did not conduct a study on correlations between imaging and pathological findings. Third, only the main three vessels were included in the vascular invasion analysis, as venous invasion is the main factor related to treatment decisions. Other affected vascular structures need to be analysed in the future.

Mono+ can improve tissue and lesion attenuation and overcome noise limitations. Further investigations should be undertaken to explore how this algorithm can reduce the radiation dose and the amount of contrast medium injection.

Conclusions

To our knowledge, this study was the first retrospective imaging data analysis of the advanced Mono+ algorithm on PDAC with a large number of patients. The objective and subjective assessments showed that Mono+ had better image quality over the conventional algorithm (i.e., Mono). Mono+ has overcome the noise limitations of the conventional Mono at energy levels < 70 keV. Based on the objective and subjective reading results, we recommend Mono+ 40 keV for the image diagnosis of PDAC.

Conflict of Interest

The Authors declare that they have no conflict of interests.

Acknowledgements

We would like to thank editage for English language editing and proofreading of the article. We also thank SIEMENS Healthcare for technical assistance and suggestions on dual-energy CT scanning and image reconstruction protocols.

References

- 1) TEMPERO MA. NCCN guidelines updates: pancreatic cancer. *J Natl Compr Canc Netw* 2019; 17: 603-605.
- 2) YU L, LENG S, MCCOLLOUGH CH. Dual-energy CT-based monochromatic imaging. *AJR Am J Roentgenol* 2012; 199: S9-S15.
- 3) MARINELLI T, FILIPPONE A, TAVANO F, FONTANA A, PELLEGRI F, KÖNINGER J, RICHTER GM, BONOMO L, BÜCHLER MW, DI SEBASTIANO P, DI MOLA FF. A tumour score with multidetector spiral CT for venous infiltration in pancreatic cancer: influence on borderline resectable. *Radiol Med* 2014; 119: 334-342.
- 4) BHOSALE P, LE O, BALACHANDRAN A, FOX P, PAULSON E, TAMM E. Quantitative and qualitative comparison of single-source dual-energy computed tomography and 120-kVp computed tomography for the assessment of pancreatic ductal adenocarcinoma. *J Comput Assist Tomogr* 2015; 39: 907-913.
- 5) ALBRECHT MH, SCHOLTZ JE, KRAFT J, BAUER RW, KAUP M, DEWES P, BUCHER AM, BURCK I, WAGENBLAST J, LEHNERT T, KERL JM, VOGL TJ, WICHMANN JL. Assessment of an advanced monoenergetic reconstruction technique in dual-energy computed tomography of head and neck cancer. *Eur Radiol* 2015; 25: 2493-2501.
- 6) FRELLESEN C, FESSLER F, HARDIE AD, WICHMANN JL, DE CECCO CN, SCHOEPP UJ, KERL JM, SCHULZ B, HAMMERSTINGL R, VOGL TJ, BAUER RW. Dual-energy CT of the pancreas: improved carcinoma-to-pancreas contrast with a noise-optimized monoenergetic reconstruction algorithm. *Eur J Radiol* 2015; 84: 2052-2058.
- 7) BELLINI D, GUPTA S, RAMIREZ-GIRALDO JC, FU W, STINNETT SS, PATEL B, MILETO A, MARIN D. Use of a noise optimized monoenergetic algorithm for patient-size independent selection of an optimal energy level during dual-energy CT of the pancreas. *J Comput Assist Tomogr* 2017; 41: 39-47.
- 8) GRANT KL, FLOHR TG, KRAUSS B, SEDLMAIR M, THOMAS C, SCHMIDT B. Assessment of an advanced image-based technique to calculate virtual monoenergetic computed tomographic images from a dual-energy examination to improve contrast-to-noise ratio in examinations using iodinated contrast media. *Invest Radiol* 2014; 49: 586-592.
- 9) HARDIE AD, PICARD MM, CAMP ER, PERRY JD, SURANYI P, DE CECCO CN, SCHOEPP UJ, WICHMANN JL. Application of an advanced image-based virtual monoenergetic reconstruction of dual source dual-energy CT data at low keV increases image quality for routine pancreas imaging. *J Comput Assist Tomogr* 2015; 39: 716-720.
- 10) CHU LC, GOGGINS MG, FISHMAN EK. Diagnosis and detection of pancreatic cancer. *Cancer J* 2017; 23: 333-342.
- 11) MACARI M, SPIELER B, KIM D, GRASER A, MEGIBOW AJ, BABB J, CHANDARANA H. Dual-source dual-energy MDCT of pancreatic adenocarcinoma: initial observations with data generated at 80 kVp and at simulated weighted-average 120 kVp. *AJR Am J Roentgenol* 2010; 194: W27-W32.
- 12) QUINEY B, HARRIS A, McLAUGHLIN P, NICOLAOU S. Dual-energy CT increases reader confidence in the detection and diagnosis of hypoattenuating pancreatic lesions. *Abdom Imaging* 2015; 40: 859-864.
- 13) GUPTA S, WAGNER-BARTAK N, JENSEN CT, HUI A, WEI W, LERTDILOK P, QAYYUM A, TAMM EP. Dual-energy CT of pancreatic adenocarcinoma: reproducibility of primary tumor measurements and assessment of

- tumor conspicuity and margin sharpness. *Abdom Radiol (NY)* 2016; 41: 1317-1324.
- 14) HE YL, ZHANG DM, XUE HD, JIN ZY. Clinical value of dual-energy CT in detection of pancreatic adenocarcinoma: investigation of the best pancreatic tumor contrast to noise ratio. *Chin Med Sci J* 2013; 27: 207-212.
 - 15) McNAMARA MM, LITTLE MD, ALEXANDER LF, CARROLL LV, BEASLEY TM, MORGAN DE. Multireader evaluation of lesion conspicuity in small pancreatic adenocarcinomas: complimentary value of iodine material density and low keV simulated monoenergetic images using multiphasic rapid kVp-switching dual energy CT. *Abdom Imaging* 2015; 40: 1230-1240.
 - 16) SCHABEL C, BONGERS M, SEDLMAIR M, KORN A, GROSSE U, MANGOLD S, CLAUSSEN CD, THOMAS C. Assessment of the hepatic veins in poor contrast conditions using dual energy CT: evaluation of a novel monoenergetic extrapolation software algorithm. *Rofo* 2014; 186: 591-597.
 - 17) AL-HAWARY MM, FRANCIS IR, CHARI ST, FISHMAN EK, HOUGH DM, LU DS, MACARI M, MEGIBOW AJ, MILLER FH, MORTELE KJ, MERCHANT NB, MINTER RM, TAMM EP, SAHANI DV, SIMEONE DM. Pancreatic ductal adenocarcinoma radiology reporting template: consensus statement of the society of abdominal radiology and the american pancreatic association. *Gastroenterology* 2014; 146: 291-304.e.1.